coatings

Article

Antifouling Coatings Fabricated by Laser Cladding

Shuwen Wang [1,*], Yang Chen [1], Chunxing Gu [1], Qingyi Sai [2,*], Tianyu Lei [3] and John Williams [4]

[1] College of Mechanical Engineering, University of Shanghai for Science and Technology, Shanghai 200093, China
[2] College of Energy and Power Engineering, University of Shanghai for Science and Technology, Shanghai 200093, China
[3] Faculty of Science, McGill University, Montreal, QC H3A 0G5, Canada
[4] Robinson College, University of Cambridge, Cambridge CB3 9AN, UK
* Correspondence: wsw@usst.edu.cn (S.W.); saiqingyi@usst.edu.cn (Q.S.)

Abstract: Laser surface treatment is a very useful technology for the fabrication of functional surfaces. In this study, novel antifouling surfaces are fabricated by laser cladding of TC4 and Ni60 mixed materials in various mass ratios on the surfaces of 316L stainless steel substrates. Parametric studies are carried out to investigate the effects of the mixed powder mass ratios and laser cladding parameters on the antifouling performance of the laser clad coatings (LCCs). The antifouling mechanism of the LCCs is investigated by using the water contact angle/surface energy measurement, scanning electron microscope (SEM) surface observation, and phase composition analysis via XRD (X-ray diffractometer) testing. The experimental results show that the LCCs with Ni60/TC4 mass ratio of 3/7 has better antifouling performance in this study. The antifouling performance of the LCC decreases with the increase in laser scanning speed. Surface energy and surface topography have a significant effect on the antifouling performance of LCCs. In order to get the optimal antifouling performance of LCCs, the Ni60/TC4 mass ratio and laser cladding parameters should be optimized.

Keywords: antifouling coating; laser cladding; microbial attachment rate; surface energy; surface topography; Ni60/TC4

check for updates

Citation: Wang, S.; Chen, Y.; Gu, C.; Sai, Q.; Lei, T.; Williams, J. Antifouling Coatings Fabricated by Laser Cladding. *Coatings* **2023**, *13*, 397. https://doi.org/10.3390/coatings13020397

Academic Editor: Domenico Pangallo

Received: 3 January 2023
Revised: 30 January 2023
Accepted: 3 February 2023
Published: 9 February 2023

1. Introduction

Biofouling is ubiquitous in the marine environment and is a major concern in the shipping industry. The growth of organisms on a vessel hull or ship increases frictional drag that reduces ship speed or requires increased power and fuel consumption to maintain its speed [1]. Slime films alone can increase powering costs by 21%, with heavy calcareous biofouling increasing the cost by up to 86% [2]. The economic costs of ship fouling have been a driving force behind the development of antifouling technologies, a growing global industry that is now worth at least USD 4 billion annually. Dafforn et al. [3] reviewed existing information regarding the ecological impact of biocides in a wide range of organisms and highlighted directions for the management of antifouling paints, and focused particularly on representatives of the recent past biocides.

Traditionally, there are three types of antifouling coatings: base material soluble antifouling paint, base insoluble antifouling paint, and organic tin self-polishing antifouling paint. However, traditional antifouling coatings release harmful substances into the sea when they are dissolved, which harms the marine environment. Therefore, a number of studies have been carried out on the development of biological antifouling coatings. Salama et al. [4] extracted the metabolites of macro-algae from the Red Sea, added them to varnish, and coated them on a nylon mesh board. Experimental results showed that the panel-attached biofouling with seaweed extract was significantly reduced. Bers et al. [5] studied the extracts from the keratin membrane of the shell of the purple mussel and found that these extracts could effectively prevent the attachment of barnacle larvae, bacteria, and algae. Guenther et al. [6] found that the surface of starfish consists of a thin layer of cuticle covered by an epidermis, which can effectively inhibit the attachment of algae, barnacles, polychaeta, bryozoans, and sea squirts. Lai et al. [7] isolated 12 compounds from soft corals, two of which had good antifouling performance.

Low surface energy antifouling coatings are also widely used in marine equipment antifouling. At present, the most widely used low surface energy coatings are mainly divided into two categories: organic fluorine and silicone. Schumacher et al. [8] prepared morphologies with different characteristic sizes, geometric shapes, and roughness on the surface of polydimethylsiloxane elastomers and studied the effects of different morphologies on the attachment of algae and spores. Qu et al. [9] prepared a new type of low surface energy antifouling coating by nano-TiO_2 modification of synthetic silicon-modified acrylic resin, which was reported to have a good antifouling effect. Qiu et al. [10] developed a number of marine antifouling coatings based on fluorocarbon copolymers. Selim et al. [11] successfully developed a novel super-hydrophobic silicone/β -MnO_2 nanorods composite for marine fouling release (FR) coatings.

In recent decades, bionic studies have shown that many organisms, such as lotus leaves, sharks, taro leaves, crabs, starfish, shells, and geckos, have self-cleaning functions due to their special surface micro-structures. Inspired by these natural self-cleaning surfaces, bionic surfaces have been fabricated, and their antifouling performance has been investigated [12–18]. In the fabrication of these bionic antifouling surfaces, various techniques were employed, such as polydimethylsiloxane (PDMS)-embedded elastomeric stamping (PEES) method [12], resin replication [13–15], electron lithography or photolithography [16], and laser surface modification [17,18].

In laser surface modification, Sun et al. [17] fabricated super-hydrophobic surfaces with controllable periodic structures on AISI304 stainless steel by a picosecond laser. They investigated their anti-biofouling performance through seawater immersion experiments for five weeks in the summertime. It was reported that a nearly 50% decrease in the average microbe attachment area ratio was obtained. Giorgi et al. [18] used a laser micro polishing technique to reduce the surface roughness and waviness of cold-rolled AISI 304 stainless steel plates and studied their surface bacteria cleanability. Experimental results showed that the laser micro polishing process was effective on bacteria cleanability.

The literature study shows that current antifouling coatings have obvious problems. On the one hand, with the continuous scouring of seawater, the concentration of the chemical coatings will be reduced, resulting in the reduction of their antifouling effectiveness. On the other hand, antifouling technology based on surface micro texturing is time-consuming and expensive, so it is difficult to apply to mass production in practice. In addition, silicone resin and fluoride resin in low surface energy antifouling coatings are too expensive because they cannot be used as a coating material alone but need to be further processed to meet the application requirements; they have poor mechanical properties and require complicated spraying operation.

In this study, a novel green antifouling method is developed by means of laser cladding technology. The solid antifouling coating fabricated by laser cladding has a long service life and efficient antifouling performance, which can be effectively applied to marine engineering, providing a feasible approach for marine antipollution and energy saving.

2. Experiment

2.1. Preparation of Antifouling Coatings

The RC-LDM8060 laser equipment (Nanjing Yuchen Laser Technology Co., Ltd., Nanjing, China) was employed for the laser cladding of the antifouling coatings in this study. The laser cladding was carried out in a closed chamber equipped with a gas circulation purification system that strictly controlled the oxygen and water to be less than 50 ppm. Figure 1 is a schematic diagram of the laser cladding treatment.

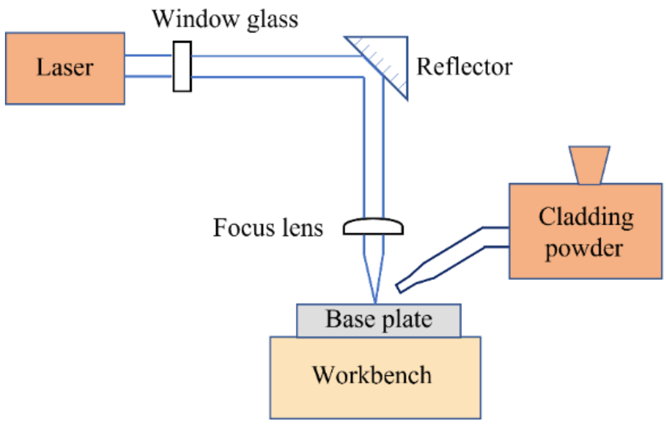

Figure 1. Schematic diagram of laser cladding.

The 316L stainless steel with a size of 350 mm × 250 mm × 5 mm was used as the substrate in this study. Mixed powders of TC4 and Ni60 were used as the laser cladding materials, as both have excellent anti-corrosion properties. The composition of TC4 (Ti6Al4V alloy) and Ni60 powders are shown in Tables 1 and 2, respectively.

Table 1. Chemical composition of TC4 (Ti6Al4V alloy) powder.

Element	Al	Fe	N	O	V	C	H	Ti
Mass fraction (%)	5.5~6.5	0.25	0.05	0.13	3.5~4.5	0.08	0.012	Bal.

Table 2. Chemical composition of Ni60 powder.

Element	C	Cr	Si	B	Fe	Ni
Mass fraction (%)	0.5	18.0	4.5	3.0	15.0	Bal.

A total of 11 specimens were prepared, including one original substrate specimen and 10 laser clad specimens with a size of 30 mm × 40 mm × 5 mm, presented in Figure 2. The material mass ratio and laser processing parameters for the laser cladding are shown in Table 3.

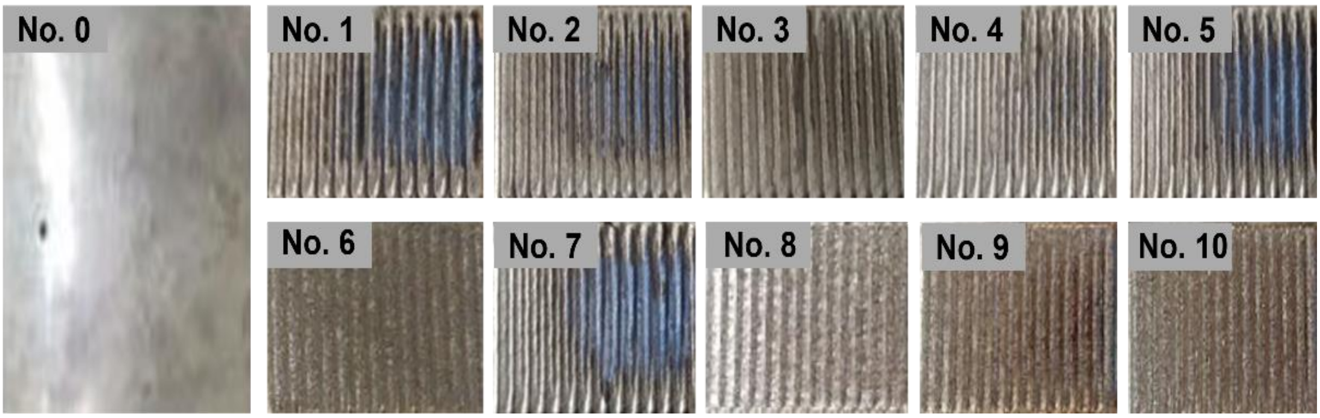

Figure 2. Laser clad coatings and the 316L stainless steel substrate.

Table 3. Mass ratio of mixed powder and laser processing parameters.

Specimen Number	Powder Mass Ratio (Ni60:TC4)	Laser Power (W)	Laser Scanning Speed (mm/min)
0	316L stainless steel	/	/
1	TC4 only	1400	1200
2	2:8	1400	1200
3	3:7	1400	1200
4	4:6	1400	1200
5	3:7	1200	1300
6	3:7	1300	1300
7	3:7	1400	1300
8	3:7	1000	1000
9	3:7	1000	1200
10	3:7	1000	1400

2.2. Experimental Methodology

2.2.1. The Microbial Attachment Testing

The eleven LCC specimens were divided into three groups, group I (specimens No. 0, 1, 2, 3, and 4), group II (specimens No. 5, 6, and 7), and group III (specimens No. 8, 9, and 10). The three groups were put into three separate beakers filled with seawater, and the three beakers were placed in a constant thermostatic water bath, as illustrated in Figure 3. The beakers were filled with seawater (from east China sea in Lingang, Pudong District, Shanghai, China) that was refreshed once a day for 40 days. Then, the specimens were taken out from the beakers for observation with fluorescence microscopy (Olympus Corporation, Tokyo, Japan). After that, the fluorescence images were processed by the ImageJ software for statistical analysis of the microbial attachments. It should be noted that the microbial colonies in the original images obtained from fluorescence microscopy are presented in blue color; they were dyed red with the ImageJ software in order to increase their clarity.

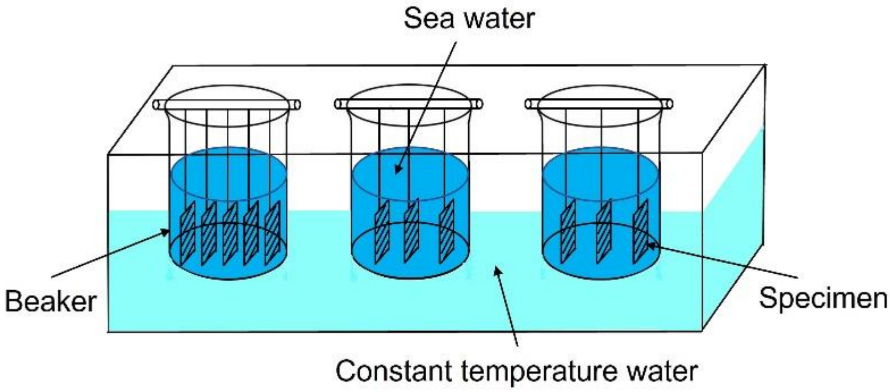

Figure 3. Micro-organism attachment experiment with seawater.

2.2.2. The Wettability Testing

The SL200B contact angle meter (made by Solon Information Technology Co., Ltd., Shanghai, China) was used to measure the contact angle and surface energy of the LCC surfaces, which is used to characterize the wettability and the antifouling mechanism of the LCC surfaces. Usually, the contact angle is measured directly, but the surface energy is calculated indirectly based on contact angle measurements with various models. In this study, Young's model, as shown in Equation (1), was used to calculate the surface energy of LCC surfaces:

$$\sigma_s = \sigma_{sl} + \sigma_l \cdot cos\theta \tag{1}$$

where σ_s is the surface energy of a solid, σ_{sl} is the interfacial tension between a liquid and a solid, σ_l is the surface tension of a liquid, and θ is the contact angle between a liquid and a solid.

2.2.3. The Mechanism of Antifouling Surface

In order to investigate the mechanism of antifouling performance of the LCCs, the Bruker D2 PHASER X-ray Diffractometer (XRD, Bruker, Billerica, MA, USA) was employed for the phase composition analysis, the SEM (Hitachi S-3400N scanning electron microscopy, Hitachi, Tokyo, Japan) was used to observe the surface topographies, and the EDS (energy dispersive spectroscopy, model 550i, IXRF, Houston, TX, USA) was used to analyze the chemical composition of the LCCs.

3. Results and Discussion

3.1. The Antifouling Performance of LCCs

3.1.1. Effect of Ni60/TC4 Mass Ratio

The microbial attachment rates of specimens group I (No. 0, 1, 2, 3, and 4) with different mixed powders of Ni60 and TC4 were observed by fluorescence microscopy. For better observation, the original blue dots in the microbial attachment images were replaced with red dots by the ImageJ software (version 1.8.0), as shown in Figure 4; while the microbial attachment rates are presented in Figure 5. The red dots shown in Figure 4 represent the micro-organisms attached to the surfaces of the specimens.

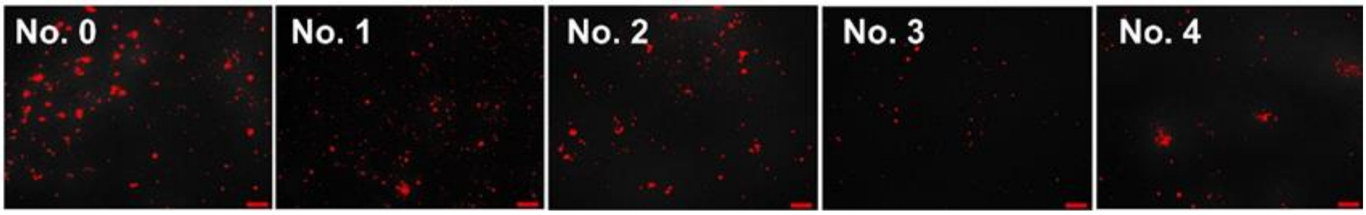

Figure 4. Images of the micro-organisms attached to specimens No. 0–4.

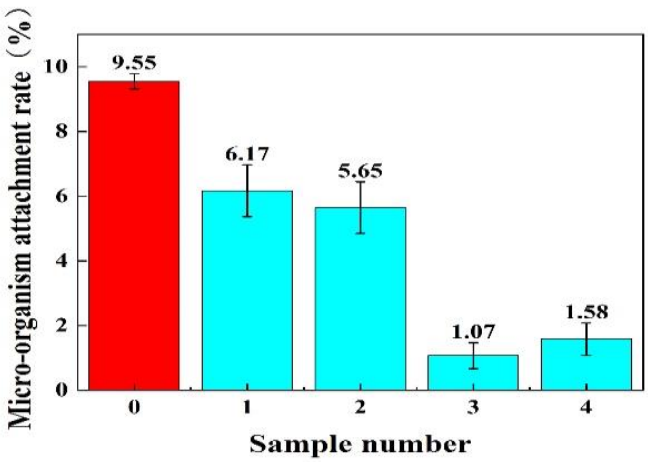

Figure 5. Micro-organism attachment rates of specimens No. 0–4.

It is observed in Figure 5 that the micro-organism attachment rates of specimens No. 1–4 are smaller than that of specimen No. 0 (originally stainless steel) and that specimen No. 3 has the minimum microbial attachment rate of 1.07% in the micro-organism attached area. As shown in Table 3, the Ni60/TC4 mass ratio of specimen No. 3 is 3/7, the laser cladding power is 1400 W, and the laser scanning speed is 1200 mm/min, indicating that with these laser cladding parameters, the specimen No. 3 has better antifouling performance or self-cleaning function than that of specimens No. 0, 1, 2, and 4.

3.1.2. Effect of Laser Cladding Power

Figure 6 shows the images of micro-organisms attached to the specimens of group II, while the microbial attachment rates of LCC specimens of group II are demonstrated in Figure 7. It is observed from Figure 7 that the LCC specimen No. 6 has the minimum microbial attachment rate of 1.56%; this specimen was processed with a laser cladding power of 1300 W, a laser scanning speed of 1300 mm/min, and a Ni60/TC4 mass ratio of 3/7. This indicates that with the laser scanning speed of 1300 mm/min, the LCC fabricated with laser cladding power of 1300 W has better antifouling performance than that of 1200 W and 1400 W. However, this conclusion may not be applied to other laser scanning speeds.

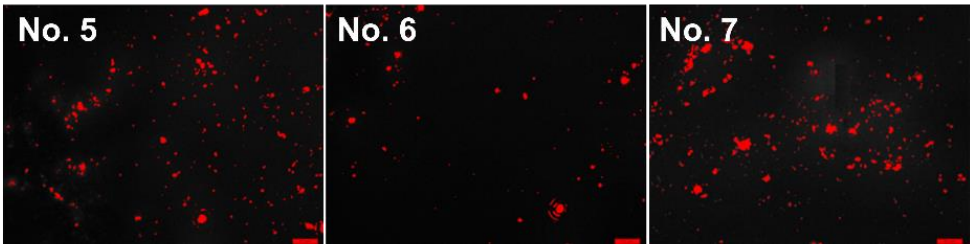

Figure 6. Images of the micro-organisms attached to specimens No. 5–7.

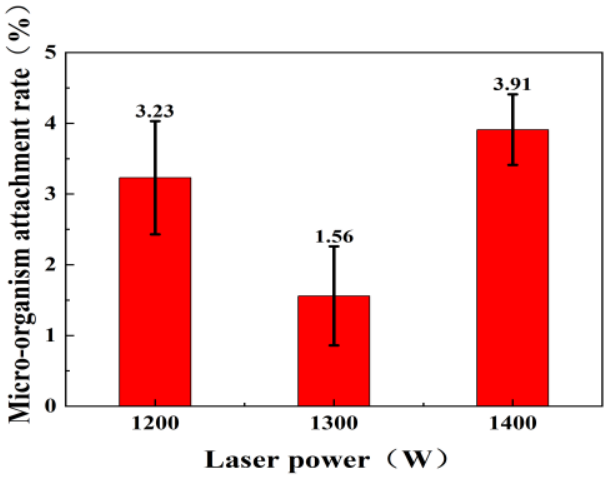

Figure 7. Micro-organism attachment rates of specimens No. 5–7.

3.1.3. Effect of Laser Scanning Speed

Figure 8 shows the images of the micro-organisms attached to the LCC specimens No. 8, 9, and 10; while the microbial attachment rates are presented in Figure 9.

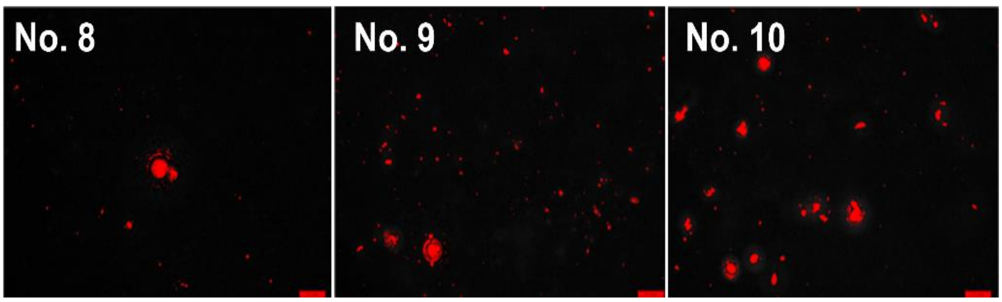

Figure 8. Images of the micro-organisms attached to specimens No. 8–10.

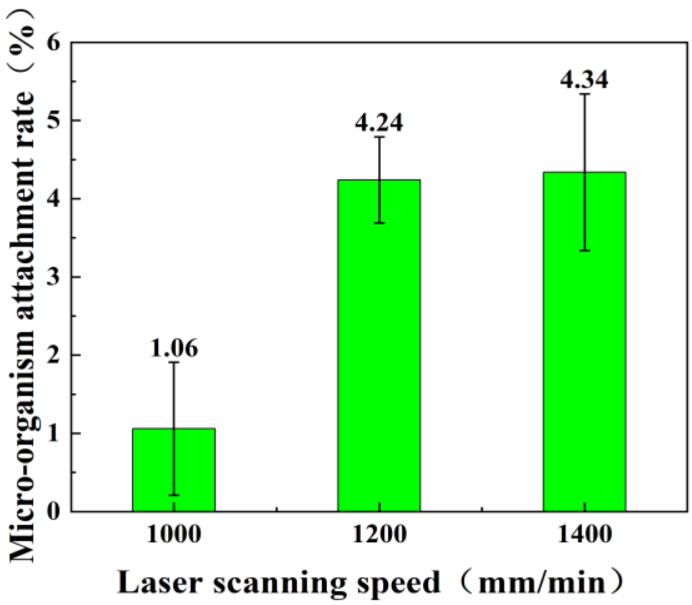

Figure 9. Micro-organism attachment rates of specimens No. 8–10.

It is observed from Figure 9 that with the same laser cladding mixed powder mass ratio and laser cladding power, the microbial attachment rate on the laser clad coating increases with increasing laser scanning speed in the range of 1000–1400 mm/min. The minimum observed microbial attachment rate is 1.06%, with a laser cladding power of 1000 W, a laser scanning speed of 1000 mm/min, and a Ni60/TC4 mass ratio of 3/7.

3.2. Wettability of LCCs

In order to investigate the antifouling mechanism of the LCCs, the wettability of the LCC specimens in terms of the water contact angle and surface energy are investigated.

3.2.1. Effect of Ni60/TC4 Mass Ratio

The contact angle measurement on each LCC specimen was repeated 5 times and averaged. Figure 10 illustrates the images of contact angle measurements, while Figure 11a,b present the measured contact angle and surface energy of LCC specimens No. 0–4, respectively.

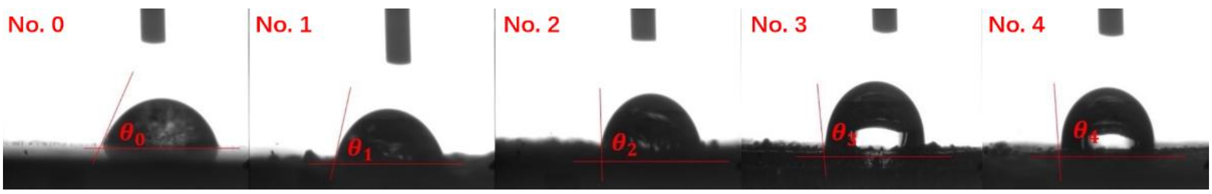

Figure 10. Contact angle measurement of LCC specimens No. 0–4.

It is observed from Figure 11 that all the surface contact angles of LCC specimens No. 1, 2, 3, and 4 are larger than that of the original specimen (316L stainless steel substrate), and the surface energy of the LCC specimens is smaller than that of the untreated material. For example, when the mass ratio of Ni60/TC4 is 3/7, the LCC has the maximum surface contact angle and the minimum surface energy. With the increasing Ni60/TC4 mass ratio in the laser cladding powder, the contact angle of the laser clad coating increased, but the surface energy decreased. However, when the mass ratio of mixed powder Ni60/TC4 is larger than 3/7, say 4/6, in this study, the surface contact angle of the LCC specimen is slightly decreased, but its surface energy is significantly increased.

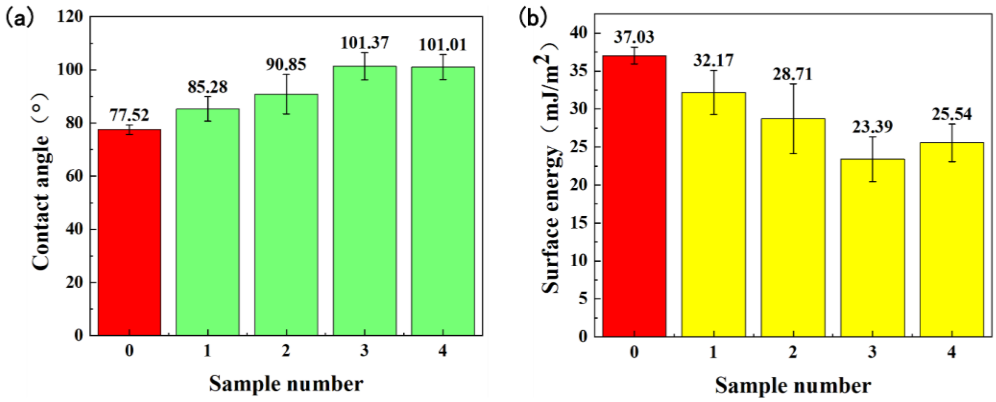

Figure 11. Measured (**a**) contact angle and (**b**) surface energy of LCC specimens No. 0–4 with various Ni60/TC4 mass ratios.

By comparing the measured contact angles and surface energies of LCC specimens No. 0–4, shown in Figure 11, with their antifouling performance, shown in Figure 5, it can be concluded that the contact angles and surface energies of the LCC surfaces are closely related to their antifouling performance and that the surface energy has a more significant correlation with the antifouling performance of the LCC surface than that of the surface contact angle. This would suggest that surface energy can be used as an important control parameter in the design of antifouling LCC surfaces.

3.2.2. Effect of Laser Cladding Power

The contact angles and surface energies of LCC specimens No. 5, 6, and 7 were measured by means of the contact angle meter, which is demonstrated in Figure 12, and the measured contact angles and surface energies of these three LCC specimens are shown in Figure 13.

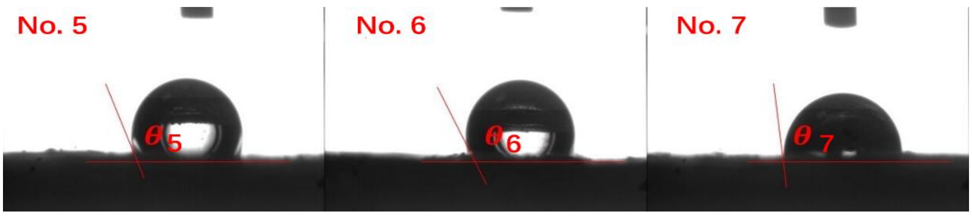

Figure 12. Contact angle measurement of LCC specimens No. 5–7.

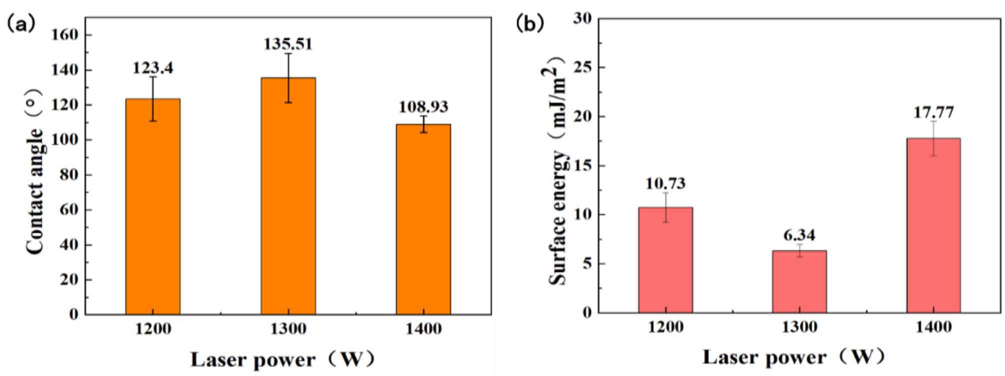

Figure 13. Measured (**a**) contact angle and (**b**) surface energy of LCC specimens No. 5–7 with Ni60/TC4 mass ratio of 3/7 and laser scanning speed of 1300 mm/min.

It is observed in Figure 13 that the LCC specimen No. 6 with the laser cladding power of 1300 W, the laser scanning speed of 1300 mm/min, and Ni60/TC4 mass ratio of 3/7 has a maximum contact angle of 135.51° and the minimum corresponding surface energy of

6.34 mJ/m^2. With increasing laser cladding power, the contact angle of laser clad coating increases first and then decreases. The surface energy decreases first and then increases, indicating that the contact angle of the LCC is not increasing linearly with laser cladding power. The effects of laser cladding power on the surface energy and the micro-organism attachment rate of the LCC specimen are very similar.

3.2.3. Effect of Laser Scanning Speed

Figure 14 illustrates the contact angle images of LCC specimens No. 8–10, and the measured contact angles are shown in Figure 15a, while the measured surface energies of these specimens are shown in Figure 15b.

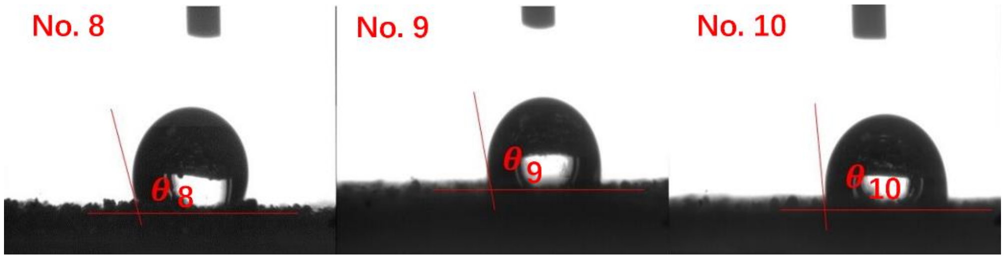

Figure 14. Contact angle measurement of LCC specimens No. 8–10.

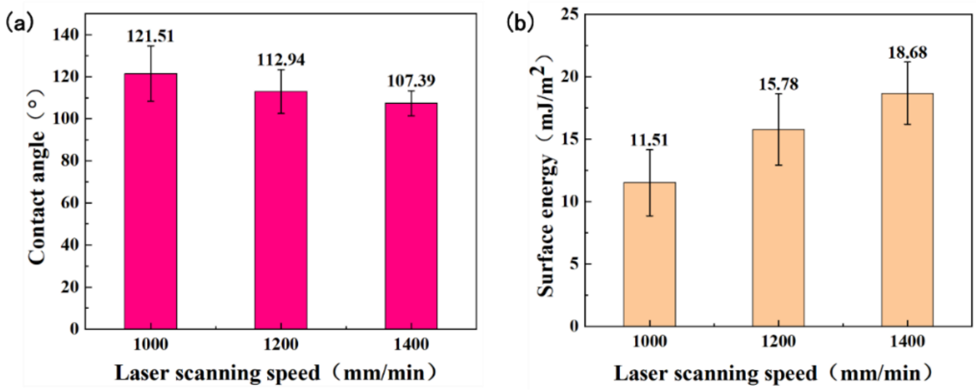

Figure 15. Measured (**a**) contact angle and (**b**) surface energy of LCC specimens No. 8–10 with Ni60/TC4 mass ratio of 3/7 and laser cladding power of 1000 W.

Figure 15 shows that the LCC specimen No. 8 has a maximum contact angle of 121.51° and a minimum corresponding surface energy of 11.51 mJ/m^2, with a laser cladding power of 1000 W, a laser scanning speed of 1000 mm/min, and a Ni60/TC4 mass ratio of 3/7. It is clearly observed that under the same mixed powder mass ratio of laser cladding material and laser cladding power, the surface contact angle of laser clad coating decreases with increasing laser scanning speed, whereas the surface energy of laser clad coating is enhanced with increasing laser scanning speed. This is consistent with the effect of laser scanning speed on the micro-organism attachment rate of the LCCs under the same conditions.

Therefore, based on the above analysis of experimental results, it may be concluded that the antifouling performance of the LCC surface is decreased with increasing laser scanning speed, as the laser and powders interacting period is shorter. Thus, fewer antifouling composites can be generated. Therefore, in order to improve the antifouling performance of LCCs, the laser scanning speed, laser cladding power, and laser cladding material mass ratio should be properly designed or optimized.

3.3. Phase Composition

In order to further investigate the antifouling mechanism of LCCs, X-ray diffractometry (XRD) was employed to analyze the phase composition of the LCC specimens in group

I with different mass ratios of Ni60/TC4 mixed powders. Figure 16 shows the phase composition analysis of the LCC specimens. It is observed in Figure 16 that a larger amount of Fe, Ni, and $FeNi_3$ composites are observed from specimens No. 3 and 4 because these two specimens have larger content of Ni60 in their mixed cladding powders. Particularly, the diffraction intensity of $FeNi_3$ in specimen 3 is larger than that of other specimens, indicating that the better antifouling performance of specimen No. 3 may attribute to the larger amount of $FeNi_3$ generated by laser cladding of the specimen, but further study is required in the future to verify this finding.

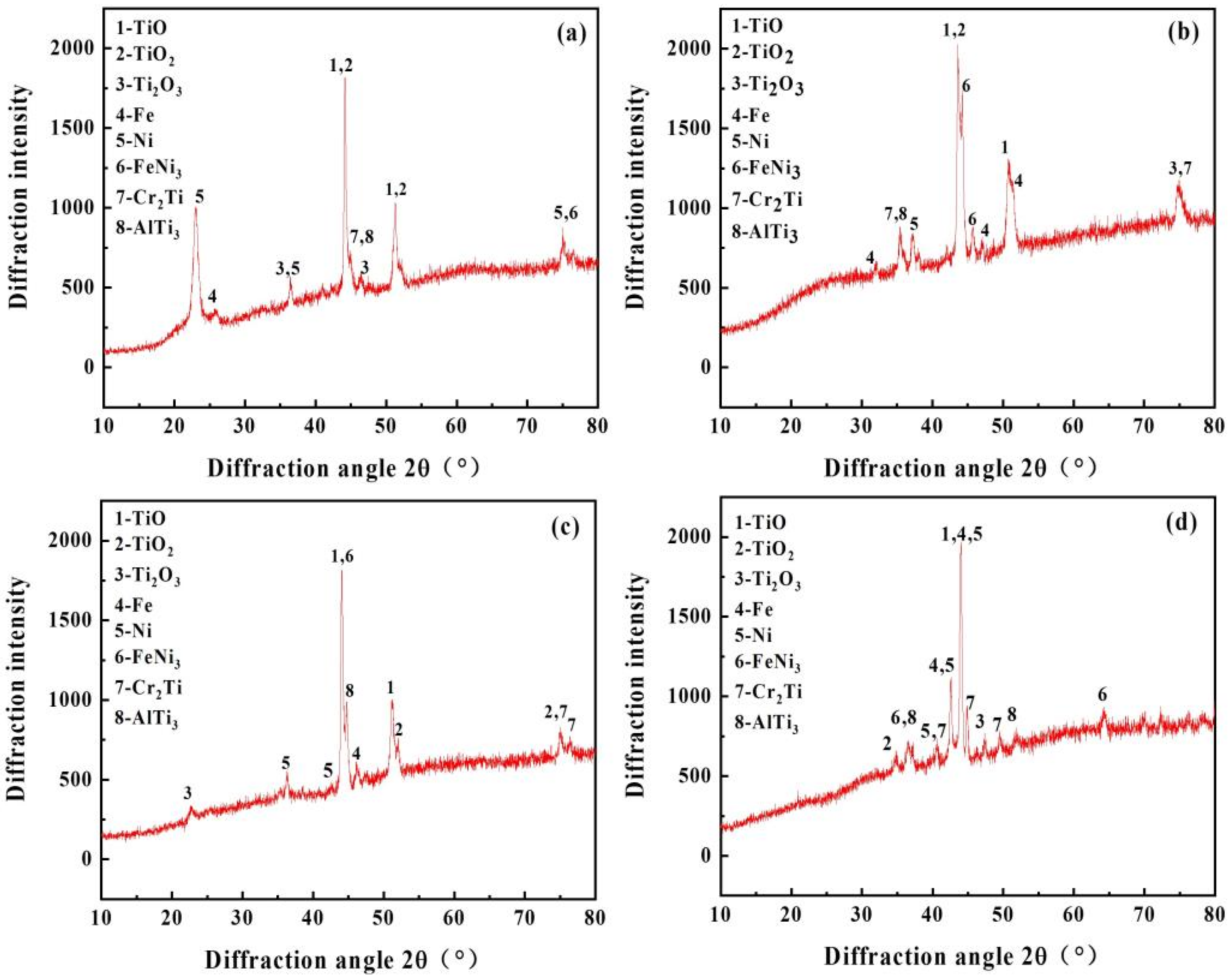

Figure 16. Analysis of phase composition of LCC specimen with various Ni60/TC4 mass ratios (**a**) No. 1 (pure TC4); (**b**) No. 2 (2/8); (**c**) No. 3 (3/7); (**d**) No. 4 (4/6).

3.4. Surface Topography

The experimental results of the micro-organism attachment rate suggest that the antifouling performance of the LCCs first increases and then decreases with an increase of Ni60 content in the mixed powder. In order to explore the reason behind this phenomenon, the surface topographies of the LCC specimens in group I were observed by scanning electron microscopy (SEM) with the combination of energy dispersive spectroscopy (EDS, model 550i) for chemical composition analysis.

Figure 17 shows the topographies of the laser clad pure TC4 coating surfaces (specimen No. 1), where macro cracks are observed in Figure 17a, and potholes with unmelted pure TC4 particles are shown in Figure 17b. Microbes in seawater can easily adhere and reproduce in the areas of macro cracks and potholes, causing the deterioration in the antifouling performance of LCC specimen No. 1.

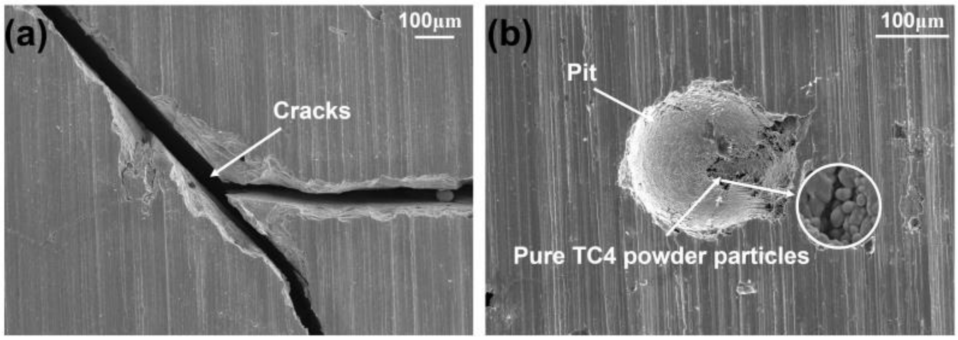

Figure 17. Surface topographies of laser clad coating (specimen No. 1). (**a**) Macro cracks; (**b**) Potholes and unmelted pure TC4 particles.

Figure 18 presents the topographies of the LCC with the Ni60/TC4 mass ratio of 2/8 (specimen No. 2). Micro cracks are also clearly observed in Figure 18a, and the black transition metal titanium carbide (TiC) is observed in Figure 18b. With the addition of Ni60 in the mixed powder for laser cladding, the cracks on the surfaces of the coating are much smaller, and the overall compactness of the LCC is improved. Compared with the pure TC4 LCC of specimen No. 1, the antifouling performance of specimen No. 2 is improved.

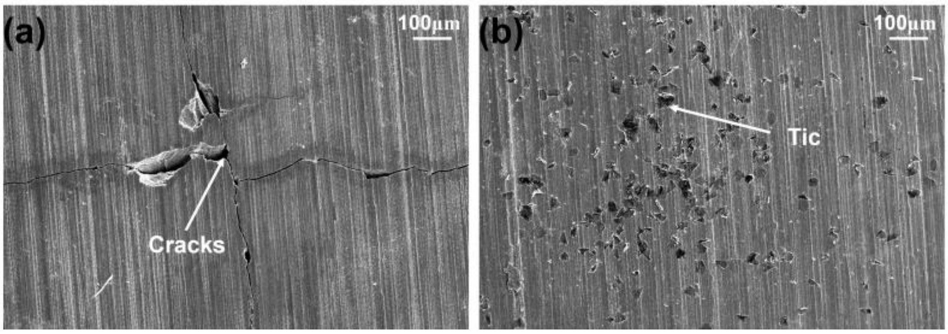

Figure 18. Surface topographies of LCC with Ni60/TC4 mass ratio of 2/8 (specimen No. 2). (**a**) Micro cracks; (**b**) Titanium carbide (TiC).

Figure 19a demonstrates the topography of LCC specimen No. 3 with a Ni60/TC4 mass ratio of 3/7. The surface of this coating is more smooth than that of specimen No. 2, without observable micro-cracks and pits under the same observation magnification as that in Figure 18. Considering that specimen No. 3 has a lower microorganism attachment rate than that of LCC specimens No. 1 and 2, it is reasonable to conclude that the surface quality (or the surface topography) of the LCC is critical to its antifouling performance.

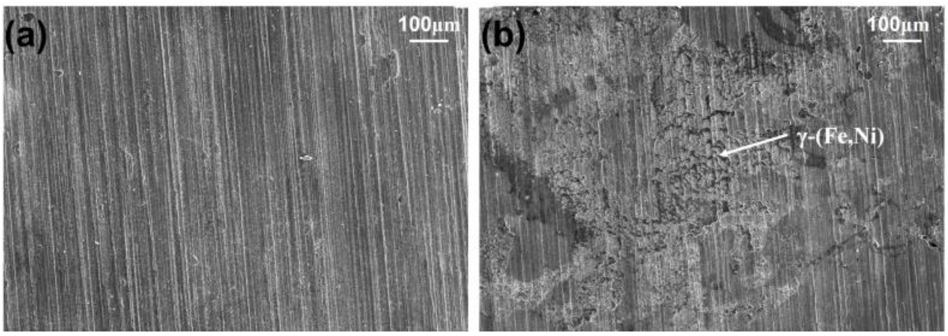

Figure 19. Surface topographies of LCC specimens. (**a**) No. 3; (**b**) No. 4.

Figure 19b shows the topography of LCC specimen No. 4 with a Ni60/TC4 mass ratio of 4/6, which is similar to that of the LCC specimen No. 3. However, due to the increase of Ni60 in the mixed laser cladding powders, a flake type of gamma (Fe, Ni) alloy has been generated by the laser cladding, and the coating surface is partially covered by this alloy. As a result, the antifouling performance of the LCC specimen No. 4 is slightly decreased, although the coating has better compactness and other mechanical properties.

It can be summarized from the above SEM analysis that properly increasing the Ni60 content in the mixed cladding powder can improve the quality of the LCC surface and thus improve its antifouling performance. However, excessive Ni60 may lead to the generation of a large amount of gamma (Fe, Ni) alloy in the coating, which may affect its antifouling performance. In order to get the optimal antifouling performance of LCCs, the Ni60/TC4 mass ratio and laser cladding parameters should be optimized.

4. Conclusions

A novel antifouling coating fabricating method is developed in this study by means of the laser cladding of mixed Ni60/TC4 powders on 316L stainless steel substrates. The effects of the laser processing parameters and the mass ratios of mixed powder on the antifouling performance of LCCs were investigated. The antifouling mechanism of LCCs was explored by the contact angle/surface energy analysis, phase composition analysis, and micro-structural observation of the LCC surfaces. The conclusions may be drawn as follows:

(1) The laser cladding parameters and mass ratios of mixed laser cladding powders have a significant effect on the contact angle, surface energy, and, thus, the antifouling performance of the LCCs. The surface energy of an LCC surface has a more significant correlation with its antifouling performance than its surface contact angle.

(2) In this study, when the Ni60/TC4 mass ratio was 3/7, the antifouling performance of LCCs were improved. Specimens 3 and 8 demonstrated the best antifouling performance but were fabricated with different laser power and scanning speeds, which indicates that the optimal antifouling surface can be obtained by properly choosing the combination of the mass ratio of laser cladding powders, laser cladding power, and laser scanning speed.

(3) The XRD analysis and SEM observation show that with increasing Ni60 content, the LCC surface has a superior quality without cracks and potholes, but larger amounts of a gamma (Fe, Ni) alloy were generated in the LCCs. In order to get the LCC with the best antifouling performance, the Ni60/TC4 mass ratio and laser cladding parameters should be optimized.

Author Contributions: Conceptualization, S.W. and Q.S.; methodology, S.W. and Q.S.; validation, S.W., Q.S. and C.G.; formal analysis, Y.C.; investigation, Y.C. and C.G.; resources, S.W. and Q.S.; data curation, S.W.; writing—original draft preparation, Y.C.; writing—review and editing, S.W., T.L. and J.W.; supervision, S.W. and Q.S.; project administration, C.G.; funding acquisition, S.W. and Q.S. All authors have read and agreed to the published version of the manuscript.

Funding: This research was partly funded by the Science and Technology Commission of Shanghai Municipal, Grant No. 18060502400, and the Natural Science Foundation of Shanghai, Grant No. 21ZR1445000.

Institutional Review Board Statement: Not applicable.

Informed Consent Statement: Not applicable.

Data Availability Statement: Not applicable.

Acknowledgments: The authors would like to thank Nanjing Yuchen Laser Technology Co., Ltd., China, for the valuable assistance in laser cladding.

Conflicts of Interest: The authors declare no conflict of interest.

References

1. Abbott, A.; Abel, P.D.; Arnold, D.W.; Milne, A. Cost-benefit analysis of the use of TBT: The case for a treatment approach. *Sci. Total Environ.* **2000**, *258*, 5–19. [CrossRef]
2. Schultz, M.P. Effects of coating roughness and biofouling on ship resistance and powering. *Biofouling* **2007**, *23*, 331–341.
3. Dafforn, K.A.; Lewis, J.A.; Johnston, E.L. Antifouling strategies: History and regulation, ecological impacts and mitigation. *Mar. Pollut. Bull.* **2011**, *62*, 453–465.
4. Salama, A.J.; Satheesh, S.; Balqadi, A.A. Antifouling activities of methanolic extracts of three macroalgal species from the Red Sea. *J. Appl. Phycol.* **2018**, *30*, 1943–1953. [CrossRef]
5. Valeria Bers, A.; D'souza, F.; Klijnstra, J.W.; Willemsen, P.R.; Wahl, M. Chemical defence in mussels: Antifouling effect of crude extracts of the periostracum of the blue mussel *Mytilus edulis*. *Biofouling* **2006**, *22*, 251–259. [CrossRef]
6. Guenther, J.; Walker-Smith, G.; Warén, A.; De Nys, R. Fouling-resistant surfaces of tropical sea stars. *Biofouling* **2007**, *23*, 413–418. [CrossRef]
7. Lai, D.W.; Geng, Z.F.; Deng, Z.W.; Ofwegen, L.V.; Proksch, P.; Lin, W.H. Cembranoids from the soft coral *Sinularia rigida* with antifouling activities. *J. Agric. Food Chem.* **2013**, *61*, 4585–4592. [CrossRef]
8. Schumacher, J.F.; Carman, M.L.; Estes, T.G.; Feiberg, A.W.; Wilson, L.H.; Callow, M.E.; Callow, J.A.; Finlay, J.A.; Brennan, A.B. Engineered antifouling micro topographies—Effect of feature size, geometry, and roughness on settlement of zoospores of the green alga *Ulva*. *Biofouling* **2007**, *23*, 55–62. [CrossRef]
9. Qu, Y.Y.; Huang, H.F. Study of novel low surface energy antifouling coating prepared with silicon-modified acrylic resin and Nano-TiO_2. *Asian J. Chem.* **2015**, *4*, 1212–1214. [CrossRef]
10. Qiu, C.H.; Qi, Y.H.; Zhang, Z.P.; Gao, H. Study on fluorocarbon antifouling coatings with low surface energy. *Mater. Sci. Forum* **2011**, *689*, 445–449.
11. Selim, M.S.; Yang, H.; El-Safty, S.A.; Fatthallah, N.A.; Shenashen, M.A.; Wang, F.Q.; Huang, Y. Super hydrophobic coating of silicone/β–MnO_2 nanorod composite for marine antifouling. *Colloids Surf. A* **2019**, *570*, 518–530.
12. Pu, X.; Li, G.J.; Huang, H.L. Preparation, anti-biofouling and drag-reduction properties of a biomimetic shark skin surface. *Biol. Open* **2016**, *5*, 389–396. [CrossRef]
13. Guenther, J.; De Nys, R. Surface micro topographies of tropical sea stars: Lack of an efficient physical defence mechanism against fouling. *Biofouling* **2007**, *23*, 419–429. [CrossRef]
14. Bai, X.Q.; Xie, G.T.; Fan, H.; Peng, Z.X.; Yuan, C.Q.; Yan, X.P. Study on biomimetic preparation of shell surface microstructure for ship antifouling. *Wear* **2013**, *306*, 285–295. [CrossRef]
15. Callow, M.E.; Jennings, A.R.; Brennan, A.B.; Seegert, C.E.; Gibson, A.; Wilson, L.; Feinberg, A.; Baney, R.; Callow, J.A. Microtopographic cues for settlement of zoospores of the green fouling alga enteromorpha. *Biofouling* **2002**, *18*, 237–245.
16. Vucko, M.J.; Poole, A.J.; Carl, C.; Sexton, B.A.; Glenn, F.L.; Whalan, S.; De Nys, R. Using textured PDMS to prevent settlement and enhance release of marine fouling organisms. *Biofouling* **2014**, *30*, 1–16. [CrossRef]
17. Sun, K.; Yang, H.; Xue, W.; He, A.; Zhu, D.H.; Liu, W.W.; Adeyemi, K.; Cao, Y. Anti-biofouling super hydrophobic surface fabricated by picosecond laser texturing of stainless steel. *Appl. Surf. Sci.* **2018**, *436*, 263–267. [CrossRef]
18. Giorgi, C.D.; Furlan, V.; Demir, A.G.; Tallarita, E.; Candiani, G.; Previtali, B. Laser micropolishing of AISI 304 stainless steel surfaces for cleanability and bacteria removal capability. *Appl. Surf. Sci.* **2017**, *406*, 199–211. [CrossRef]